THz wave transmission within the metal-clad antiresonant reflecting hollow waveguides

Jiamin Liu,[1,2,3] Huawei Liang,[2,3,*] Min Zhang,[2,3] and Hong Su[2,3]

[1]*College of Electronic Science and Technology, Shenzhen University, Shenzhen, 518060, China*
[2]*Shenzhen Key Laboratory of Laser Engineering, Shenzhen University, Shenzhen, 518060, China*
[3]*Key Laboratory of Advanced Optical Precision Manufacturing Technology of Guangdong Higher Education Institutes, Shenzhen University, Shenzhen, 518060, China*
**Corresponding author: hwliang@szu.edu.cn*

Abstract: We present the transmission characteristics of THz waves in the metal-clad antiresonant reflecting hollow waveguides. We have derived the equation for the blueshift of the resonance frequency. The effects of the waveguide structure on the blueshift of the resonance frequency are studied comprehensively. In particular, we find that the blueshift of the resonance frequency is strongly affected by the interval between two dielectric slabs. By changing the interval, we obtain that the maximum frequency-tuning-range is up to 2030 GHz, and the maximum sensitivity of the resonance frequency shift is up to 6950 GHz/mm at the resonance order of *m* = 1. When the THz wave is at the near-zero loss frequency, both the loss and the dispersion of the guide modes are very low. ©2015 Optical Society of America

OCIS codes: *(260.3090) Infrared, far; (230.7370) Waveguides; (230.7390) Waveguides, planar.*

1. Introduction

In recent years, THz waveguides [1,2] have attracted much attention, such as metal wire waveguides [3-5], dielectric pipe waveguides [6-9], ultra-thin metal pipe waveguides [10], and terahertz porous fibers [2, 11-14]. And they have been widely used in communications, spectroscopy, imaging and sensing. The functional devices [15,16] such as THz switches [17,18], filters [15,18-21] and THz sensors [22-24] are hot research topics. Recently, much attention has been paid to low loss planar THz waveguides [25,26], such as parallel plate waveguides [25, 27-29], metal nanofilm waveguides [30], metal-clad antiresonant reflecting hollow waveguides [20], and single metal plate waveguides [31-34]. And more articles have reported switches, filters [15, 19-21], sensors [24, 31-34] based on the planar THz waveguides for their simple structure. Lu et al. proposed the metal-clad antiresonant reflecting hollow waveguide for the tunable filter application [20]. They studied the antiresonant reflecting mechanism of the waveguide experimentally and supported by numerical simulations.

In this paper, we analytically study the transmission characteristics of the THz wave in the metal-clad antiresonant reflecting hollow waveguides. We first derive the dispersion equation of the waveguide. Then by using the dispersion equation, we study the effects of the waveguide structure on the resonance frequency comprehensively. We have also derived the equation for the blueshift of the resonance frequency. We find that the effects of the dielectric slab thickness on the resonance frequency can be predicted by the equation in [35]. The effects of the interval between the metal plate and dielectric slab on the blueshift of the resonance frequency have been discussed by Lu et al., but they did not study the effects of the interval between two dielectric slabs on the blueshift [20]. However, we find that the interval between two dielectric slabs strongly affects the blueshift of the resonance frequency. By changing this interval, we obtain that the maximum frequency-tuning-range and the maximum frequency shift sensitivity are up to 2030 GHz and 6950 GHz/mm, respectively, which are 33 times and 60 times larger than those caused by the interval between the metal plate and dielectric slab. Moreover, both the loss and the dispersion of guide modes are very low when the THz wave is at the near-zero loss frequency. We believe that the results obtained are very useful for designing THz filters, sensors and switches.

2. The dispersion equation of the metal-clad antiresonant reflecting hollow waveguide

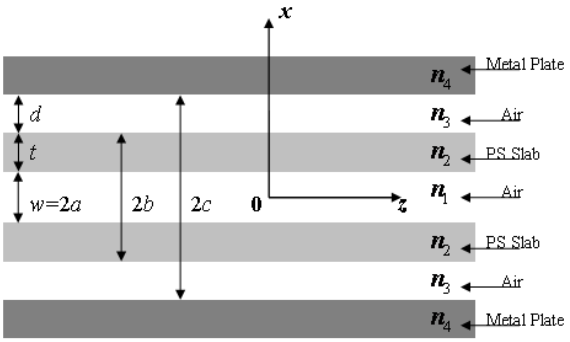

Fig. 1. The structure of the metal-clad antiresonant reflecting hollow waveguide.

The waveguide structure and coordinate system are shown in Fig. 1, and the waveguide width in *y* direction is infinity. The interval between the two Polystyrene (PS) slabs is $w = 2a$, the thickness of the PS slab is $t = b - a$, and the interval between the metal plate and PS slab is $d = c - b$. According to the traditional waveguide theory, for transverse electric (TE) modes propagating in the positive z-direction, the transverse electric field of even modes in different regions can be written as [36]:

$$E_y(x) = \begin{cases} A_{10}e^{-h_4(x-c)} & x \ge c \\ A_6 e^{-h_3(x-b)} + A_7 e^{h_3(x-b)} & b \le x \le c \\ A_2 \cos h_2(x-a) + A_3 \sin h_2(x-a) & a \le x \le b \\ A_1 \cos(h_1 x) & -a \le x \le a \\ A_4 \cos h_2(x+a) + A_5 \sin h_2(x+a) & -b \le x \le -a \\ A_8 e^{-h_3(x+b)} + A_9 e^{h_3(x+b)} & -c \le x \le -b \\ A_{10}e^{h_4(x+c)} & x \le -c \end{cases} \quad (1)$$

where A_1 ~ A_{10} are unsolved mode coefficients in different regions, $h_1 = (n_1^2 k_0^2 - \beta^2)^{1/2}$, $h_2 = (n_2^2 k_0^2 - \beta^2)^{1/2}$, $h_3 = (\beta^2 - n_3^2 k_0^2)^{1/2}$, and $h_4 = (\beta^2 - n_4^2 k_0^2)^{1/2}$. The complex variable of β is $\beta = \beta_1 - j*\alpha$, in which the real part β_1 is related to the effective refractive index $n_{eff} = \beta_1 / k_0$ and the imaginary part α is the loss coefficient of the mode. The wave vector in vacuum is $k_0 = 2\pi/\lambda$, and n_1, n_2, n_3, and n_4 are refractive indices of air, the PS slab, air and the metal plate, respectively. According to Eq. (1), we derive the longitudinal magnetic field of the modes by using $H_z(x) = \frac{j}{\omega\mu}\frac{\partial}{\partial x}E_y(x)$. Then basing on the continuities of tangential field components at the interfaces, we further derive the following dispersion equation:

$$\tan(h_1 a) = \frac{P_1 + P_2}{P_3 + P_4} \quad (2)$$

where $P_1 = [1 + \frac{h_2}{h_3}\tan h_2(b-a) - \frac{h_3}{h_4} - \frac{h_2}{h_4}\tan h_2(b-a)]e^{-h_3(c-b)}$,

$P_2 = [1 - \frac{h_2}{h_3}\tan h_2(b-a) + \frac{h_3}{h_4} - \frac{h_2}{h_4}\tan h_2(b-a)]e^{h_3(c-b)}$,

$P_3 = [-\frac{h_3}{h_4}\frac{h_1}{h_2}\tan h_2(b-a) + \frac{h_1}{h_4} + \frac{h_1}{h_2}\tan h_2(b-a) - \frac{h_1}{h_3}]e^{-h_3(c-b)}$, and

$P_4 = [\frac{h_3}{h_4}\frac{h_1}{h_2}\tan h_2(b-a) + \frac{h_1}{h_4} + \frac{h_1}{h_2}\tan h_2(b-a) + \frac{h_1}{h_3}]e^{h_3(c-b)}$.

Copper is adopted as the material of the metal plates, and its relative permittivity $\varepsilon_4 = n_4^2$ can be gotten according to the Drude model:

$$\varepsilon_4 = \varepsilon_\infty - \frac{\omega_p^2}{\omega^2 - j\omega\omega_\tau} \quad (3)$$

where ω is the angular frequency of the THz wave, ε_∞ is the high frequency permittivity of copper, which is always negligible in the THz region, and $\omega_p = 1.1234\times10^{16}$ Hz and $\omega_\tau = 1.3798\times10^{13}$ Hz are the plasma oscillation frequency and damping frequency of copper [37], respectively. According to Eq. (3), we can obtain the refractive index of copper. The material of dielectric slabs is Polystyrene (PS) with a refractive index of $n_2 = 1.58 - j0.0036$ [38]. The refractive index of air is $n_1 = n_3 = 1$.

3. The transmission characteristics of the metal-clad antiresonant reflecting hollow waveguide

3.1 The loss, dispersion and mode field distribution

When the interval between the two PS slabs is w = 8 mm, the thickness of the PS slabs is t = 1 mm, and the interval between the metal plate and PS slab is d = 5 mm, we numerically calculate the dependence of the loss coefficient on the THz frequency by Eq. (2), as shown in Fig. 2(a). From Fig. 2(a), we can observe that the mode loss is very low when the THz wave is far away from the resonance frequency (for example, $\alpha = 0.00022\ \mathrm{cm}^{-1}$ at f = 0.31 THz), but increases sharply near the resonance frequency. The resonance frequency can be predicted by the following relation [35]:

$$f_{mo} = \frac{m\mathrm{c}}{2t\sqrt{n_2^2 - 1}} \tag{4}$$

where $\mathrm{c} = 3\times10^{11}\,\mathrm{mm/s}$ is the speed of light in vacuum. When the PS slab thickness is t = 1 mm, and its refractive index is $n_2 = 1.58$, according to Eq. (4) we get that the theoretical resonance frequencies are 0.123 THz, 0.245 THz, and 0.368 THz at the resonance orders m = 1, 2, and 3, respectively. The corresponding resonance frequencies obtained by the numerical calculation are 0.182 THz, 0.278 THz, and 0.390 THz, which means that the resonance frequencies show blueshifts relative to the theoretical values.

In order to get a better understanding of this mode, we calculate the mode field distributions at the lowest loss point (namely at the nearly-zero loss frequency) and the highest loss point (namely at the resonance frequency), at m = 3, as shown in Fig. 2(b) and 2(c), respectively. We first obtain the complex variable β by solving Eq. (2), and derive the relationships of the mode coefficients $A_1 \sim A_{10}$ by using the continuities of tangential field components at the interfaces. Then according to β and the relationships of $A_1 \sim A_{10}$, we further obtain the mode field distributions. From Fig. 2(c), we can see that when the THz wave is at the resonance frequency, a much larger part of the THz energy comes into the PS slabs with a high absorption loss, thus the mode loss is very high. However, when the THz wave is at the near-zero loss frequency, the field amplitude is very small in the PS slabs, as shown in Fig. 2(b), so very little THz energy propagates in the PS slabs and then the mode loss is very low. This mainly results from that most of the THz energy is reflected on the interfaces between air and the PS slabs. The blueshift of the resonance frequency can also be explained by the mode field distribution. As we can see in Fig. 2 (c), in the range of $|x| \le a$, the mode field is changing in exponent. According to Eq. (1), the field in the middle air interval is $A_1 \cos[(n_1^2 k_0^2 - \beta^2)^{1/2} x]$, so at $x = a$, we can get:

$$\sqrt{n_1^2 k_0^2 - \beta^2}\, a = jp\pi \tag{5}$$

where p is a constant which is related to the structure of the waveguide. For each resonance order m, the total phases in PS slabs at the shifted resonance frequency is $(m + l)\pi$, so:

$$\sqrt{n_2^2 k_0^2 - \beta^2}\, t = (m + l)\pi \tag{6}$$

where l is a constant which is related to d (l = 0.5 for $d = 0$, and $l = 0$ for $d \to \infty$). When d is between 0 and infinity, l is between 0 and 0.5, but the numerical calculation results show that we can adopt $l = 0$ for $d > \lambda/2$. According to Eqs. (5), (6) and $k_0 = 2\pi f_m / \mathrm{c}$, the shifted resonance frequency can be predicted by the following relation:

$$f_m = \frac{\mathrm{c}}{2\sqrt{n_2^2 - 1}} \sqrt{\left(\frac{m + l}{t}\right)^2 + \left(\frac{p}{a}\right)^2} \tag{7}$$

We substitute t = 1 mm, a = 4 mm, and $l = 0$ to Eq. (7), when m = 1, the shifted resonance frequency by numerical calculation is f = 0.182 THz, so we get the p = 4.387 for this structure. By using the proper p = 4.387 , we obtain that the resonance frequencies for m = 2 and 3 are 0.279 THz and 0.391 THz, respectively. The theoretical results are in good agreement with the numerical values.

According to Eqs. (4) and (7), the theoretical blueshift of the resonance frequency of the waveguide can be written as:

$$\Delta f = f_m - f_{mo} = \frac{\mathrm{c}}{2\sqrt{n_2^2 - 1}} \left[\sqrt{\left(\frac{m + l}{t}\right)^2 + \left(\frac{p}{a}\right)^2} - \frac{m}{t} \right] \tag{8}$$

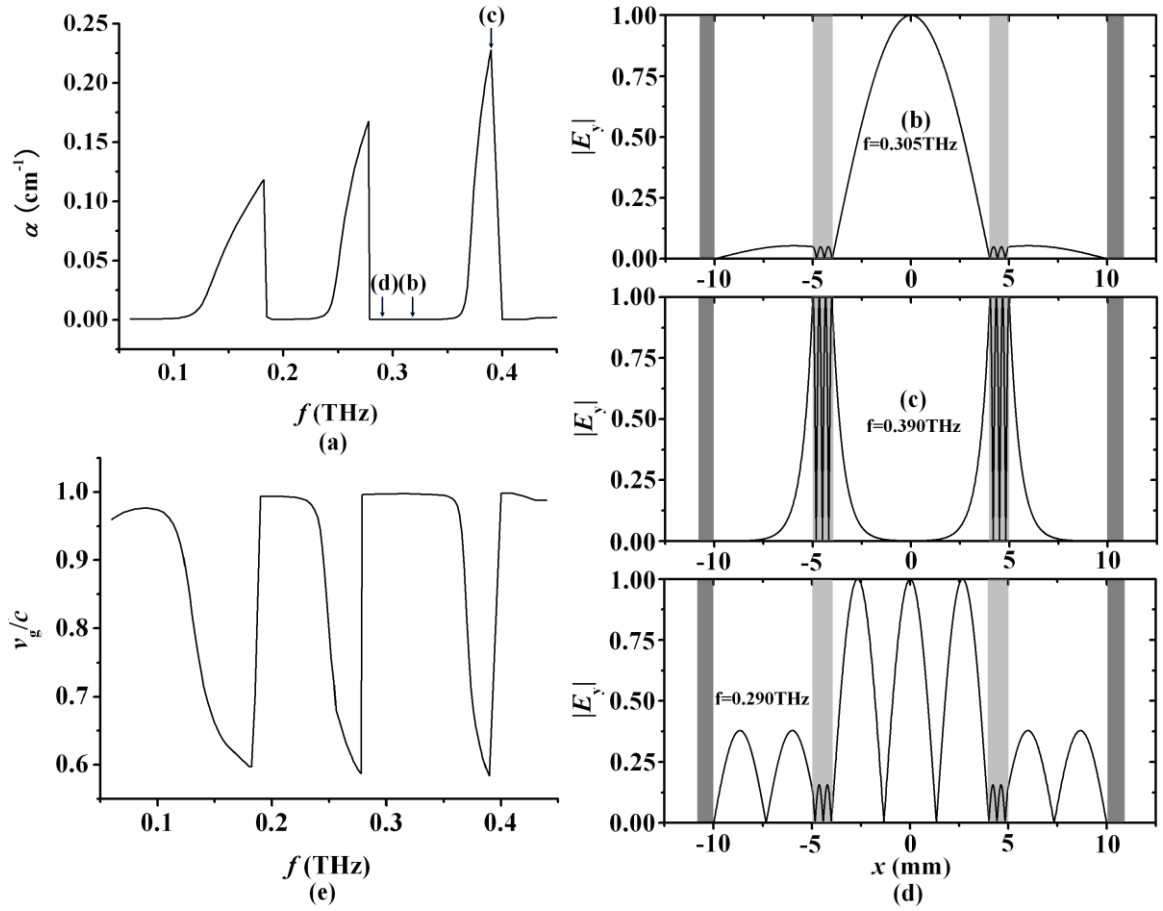

Fig. 2. (a) The dependence of the loss coefficient on the THz frequency. The curve from left to right corresponds to the resonance order of m = 1, 2, or 3. (b) and (c) are mode field distributions at the nearly-zero loss frequency and resonance frequency, respectively, at m = 3. The grey regions are the PS slabs, and the dark regions are the metal plates. (d) The mode field distribution of the higher order mode at f = 0.290 THz. (e) The dependence of the group velocity on the THz frequency.

The lowest order guided mode of the waveguide also has a near-zero loss frequency. Here we particularly point out that the order of the guided mode is independent of the resonance order. When the THz wave tends to the near-zero loss frequency, the mode loss $\alpha \to 0$. Then according to the mode field distributions, we can get the near-zero loss conditions of the lowest mode as follows:

$$\sqrt{n_1^2 k_0^2 - \beta_1^2}\, a = \pi / 2 \qquad \textbf{(9)}$$

Eq. (9) is gotten because at the point of $x = a$, the mode field is nadir, as seen in Fig. 2 (b). The phase is a real number because β is a real number for $\alpha \to 0$, which makes the field in the hollow interval change in a cosine form. While in Eq. (5), the phase is not a real number for the field in the hollow interval changes in an exponent form. According to the total phases in the PS slabs, we can also get:

$$\sqrt{n_2^2 k_0^2 - \beta_1^2}\, t = (m - 0.5 + l)\pi \qquad \textbf{(10)}$$

According to Eqs. (9) and (10), the near-zero loss frequency can be predicted by the following relation:

$$f_o = \frac{\mathrm{c}}{2\sqrt{n_2^2 - 1}} \sqrt{\left(\frac{m - 0.5 + l}{t}\right)^2 - \left(\frac{1}{2a}\right)^2} \qquad \textbf{(11)}$$

For each resonance order m, when the frequency of the THz wave is smaller than the near-zero loss frequency, the lowest order guided mode disappears, but a higher order mode appears. Therefore, we can obtain the complete transmission window, as shown in Fig. 2(a). The mode field distribution of the higher order mode at f = 0.29 THz is shown in Fig. 2(d). From Fig. 2(d), one can see that the total phase in the air core is 3π, which is different from that of the lowest order mode shown in Fig. 2(b). The total phase in each PS slab is a little larger than 2π, which indicates that this mode is near the start of the antiresonant reflecting mode of m = 3. However, in the previous study [20], the mode field distribution of the higher order mode for a given m is not given.

We substitute t = 1 mm, a = 4 mm, and $l_1 = 0.5$ to Eq. (11), and obtain that the near-zero loss frequencies of the lowest order mode are 0.0594 THz, 0.183 THz and 0.306 THz at m = 1, 2, and 3, respectively. The corresponding near-zero loss frequencies obtained by the numerical calculation are 0.0600 THz, 0.185 THz, and 0.305 THz. Therefore, the theoretical results are in good agreement with the numerical values. According to Eqs. (7) and (11), the theoretical shifted bandwidth of the transmission window of the lowest order mode in the waveguide can be written as:

$$\delta f = f_m - f_o = \frac{\mathrm{c}}{2\sqrt{n_2^2 - 1}}\left[\sqrt{\left(\frac{m+l}{t}\right)^2 + \left(\frac{p}{a}\right)^2} - \sqrt{\left(\frac{m-0.5+l}{t}\right)^2 - \left(\frac{1}{2a}\right)^2}\right] \qquad (12)$$

According to Eq. (12), we get that the theoretical shifted bandwidths of the lowest order mode are 0.123 THz, 0.0960 THz, and 0.0850 THz at m = 1, 2, and 3, respectively. The corresponding shifted bandwidths of the lowest order mode obtained by the numerical calculation are 0.122 THz, 0.0930 THz and 0.0843 THz. The numerical calculation results are in good agreement with the theoretical results. From Figs. 2(b) and 2(c), we can see that when d = 5 mm, metal plates still affect the mode field distribution in the non-resonance case, but hardly affect the mode field distribution in the resonance case. In fact, when d is larger than 1.5 mm for the given waveguide structure, the effect of copper plates on the resonance mode is very small.

According to the formula $v_g = \dfrac{c}{n_{eff}\left(1 + \dfrac{k_0}{n_{eff}}\dfrac{\mathrm{d}n_{eff}}{\mathrm{d}k_0}\right)}$, we calculate the dependence of the group velocity of guided modes on the frequency f, as shown in Fig. 2(e). From Fig. 2(e), one can know that when the THz wave is far from the resonance frequency, the group velocity is near the speed of light in vacuum and the group velocity dispersion (GVD) is very low. However, the group velocity decreases quickly near the resonance frequency, and this is because much more THz wave energy is in the PS slabs.

When d = 0 mm, 0.3 mm, and 0.5 mm, we calculate both the dependences of loss coefficients on the THz frequency and the mode field distributions at the resonance frequencies at m = 3, as shown in Fig. 3. From Fig. 3(a), we can see that for a given resonance order m, the smaller d is, the larger the resonance frequency is. When d = 0 mm, the resonance frequency obtained by the numerical calculation is 0.218 THz, 0.326 THz, or 0.442 THz at m = 1, 2, or 3, where blueshifts are found relative to the theoretical values predicted by Eq. (4). When d = 0 mm, the near-zero loss frequency of the lowest order mode obtained by the numerical calculation is 0.122THz, 0.245THz, or 0.368 THz at m = 1, 2, or 3. According to Eq. (11), we get that the corresponding theoretical near-zero loss frequency of the lowest order mode is 0.122 THz, 0.245 THz, or 0.368 THz. The numerical calculation results are in good agreement with the theoretical results. The shifted bandwidths of the lowest order mode are 0.0960 THz, 0.0810 THz, and 0.0740 THz, corresponding to m = 1, 2, and 3 for d = 0. According to the numerical calculation, the bandwidth of the lowest order mode decreases as d decreases from 5 mm to 0 mm for each m. When d decreases from 0.5 mm to 0 mm, the total phase of the electric field in the PS slab increases from 3π to 3.5π for m = 3, as shown in Fig. 3(b), which means l in Eq. (8) increases from 0 to 0.5. The increased phases cause the blueshifts of the resonance frequencies as seen in Eq. (8). Moreover, the loss at the resonance frequency increase as d decreases, as shown in Fig. 3(a). The minimum loss, which happens at the near-zero loss frequency, can be as low as $0.00019\,\mathrm{cm}^{-1}$ at d = 0 mm and f = 0.37 THz.

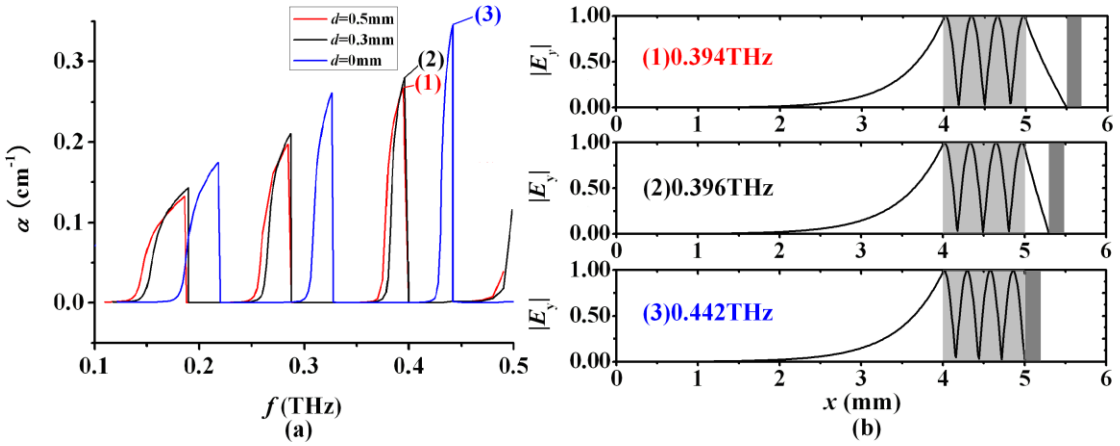

Fig. 3. (a) Dependences of the loss coefficients on the THz frequency for d = 0 mm (blue line), d = 0.3 mm (black line), or d = 0.5 mm (red line). The curve from left to right corresponds to the resonance order of m = 1, 2, or 3. (b) Mode field distributions at the resonance frequencies for m = 3. The inset (1) corresponds to d = 0.5 mm and f_m = 0.394 THz, the inset (2) corresponds to that d = 0.3 mm and f_m = 0.396 THz, and the inset (3) corresponds to that d = 0 mm and f_m = 0.442THz.

When d = 0.3 mm, w = 8 mm, and f = 0.3 THz, we numerically calculate the dependence of the loss coefficient on the PS slab thickness t based on Eq. (2), and the mode field distributions are also given at both the lowest loss thickness and the highest loss thickness at m = 2, as shown in Fig. 4. From Fig. 4(a), we can observe that when the slab thickness t tends to the resonance thickness, the mode loss increases sharply. The resonance thickness obtained by the numerical calculation is 0.479 mm, 0.890 mm, 1.30 mm, 1.71 mm, or 2.12 mm at m = 1, 2, 3, 4, or 5. According to Eq. (4), the corresponding theoretical resonance thickness is 0.409 mm, 0.817 mm, 1.23 mm, 1.64 mm, or 2.04 mm. The numerical results are larger than the theoretical values, and this difference results from the blueshifts of the resonance frequencies. It is worth to point out that when t is smaller than 0.257 mm, 0.665 mm, 1.07 mm, 1.48 mm, or 1.89 mm for each m, the lowest order mode disappears, but the higher order mode appears. This phenomenon is related to the near-zero loss frequencies. The theoretical near-zero loss thicknesses can be predicted by Eq. (11). When $d > \lambda / 2$, we can adopt l = 0 in this equation. When $d < \lambda / 2$, we should adopt a proper l according to the numerical calculation. For example, when $f_c = 0.3\,\mathrm{THz}$, w = 8 mm, and d = 0.3 mm, we can choose l = 0.13, and then we obtain that the theoretical near-zero loss thickness is 0.257 mm, 0.665 mm, 1.07 mm, 1.48 mm, or 1.89 mm, at m = 1, 2, 3, 4, or 5. The numerical results are in good agreement with the theoretical results. Comparing Fig. 4(b) with Fig. 4(c), the total phases of oscillatory electric fields in the slabs are slightly larger than 1.5π and 2π, respectively, at m = 2, which tells us that l is more than 0. When the 0.5π phase is added in the PS slab, the low loss mode is changed into the high loss mode. What is more, the loss at the resonance frequency increases as t increases. The minimum loss can be as low as $0.000071\mathrm{cm}^{-1}$ at t = 0.257 mm (the near-zero loss thickness).

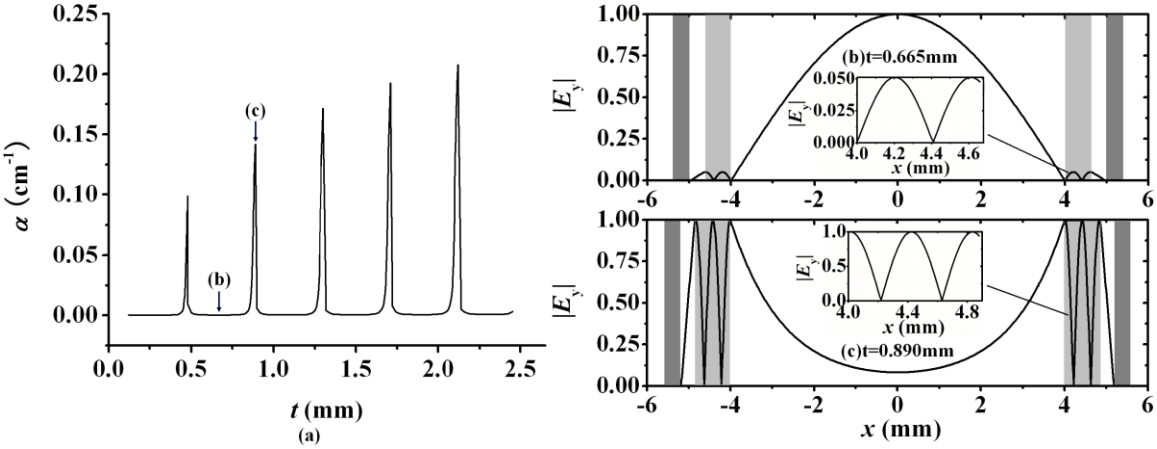

Fig. 4. (a) The dependence of the loss coefficient on the PS slab thickness. The curve from left to right corresponds to m = 1, 2, 3, 4, or 5. (b) and (c) are mode field distributions at the lowest loss thickness t = 0.665 mm and the highest loss thickness t = 0.890 mm, respectively, at m = 2. The insets in (b) and in (c) both show the corresponding mode field distributions in the PS slab.

3.2 The shift of the resonance frequency Δ*f*

When w = 8 mm, t = 1 mm, and d = 0.3 mm, we calculate the dependence of the blueshift of the resonance frequency of the waveguide Δf on the resonance order m, as shown in Fig. 5. When m increases, the blueshift of the resonance frequency decreases, and tends to a stable value gradually. From Eq. (8), we can see that for the structure of the waveguide does not change in this case, Δf will decrease when m increases. When m = 1, the blueshift of the resonance frequency is up to 67.2 GHz.

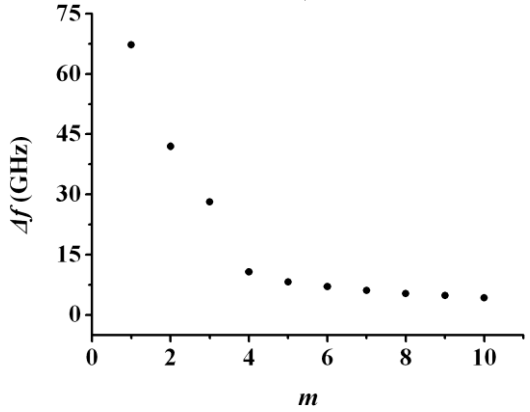

Fig. 5. The dependence of the resonance frequency shift relative to the theoretical value on the resonance order.

When w = 8 mm, d = 0.3 mm, and m = 1, we calculate the dependence of Δf on the PS slab thickness t, as shown in Fig. 6. From Fig. 6(a), one can see that when the PS slab thickness increases, the blueshift of the resonance frequency is nearly

unchanged, and always about 66 GHz. According to the mode field distributions shown in Fig. 6(b), one can know that the increasing of the slab thickness results in the increasing of the total phase in each PS slab, which tells us that both l and p in Eq. (8) will change. However, from Fig. 6 (b), we can know when t increases, l increases for the phase of the mode field on the right boundary of the slab decreases, at the same time, p decreases for the phase of the mode field on the left boundary of the slab decreases. According to Eq. (8), the blueshift of the resonance frequency is basically unchanged. Therefore, Eq. (4) in reference [35] can predict the effects of the PS slab thickness on the resonance frequency. However, the resonance frequency is also affected by w and d, which is not included in Eq. (4).

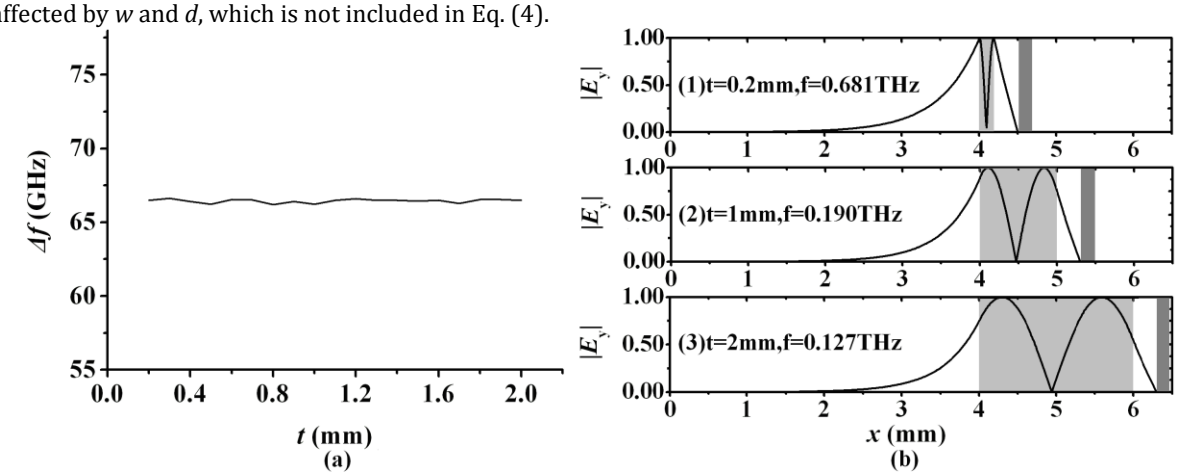

Fig. 6. (a) The dependence of the resonance frequency shift relative to the theoretical value on the PS slab thickness. (b) Mode field distributions at different slab thicknesses for m = 1. The inset (1) corresponds to t = 0.2 mm and f_m = 0.681 THz, the inset (2) corresponds to t = 1 mm and f_m = 0.190 THz, and the inset (3) corresponds to t = 2 mm and f_m = 0.127 THz.

When w = 8 mm, t = 1 mm, and m = 1, we calculate the dependence of Δf on d by the numerical calculation, as shown in Fig. 7. From Fig.7, we can observe that the blueshift of the resonance frequency decreases as d increases. This is because when d changes from 0 to infinity, in Eq. (8), only l will change (from 0.5 to 0). However, when d is large enough, l is nearly unchange (l = 0), so when d is larger than 1.5 mm, the blueshift is almost unchanged. The maximum frequency-tuning-range obtained by changing d is 37.0 GHz. The sensitivity of Δf to d is defined as $\Delta(\Delta f)/\Delta d$, where $\Delta(\Delta f)$ and Δd are the variations of Δf and d, respectively. When d is small enough, the sensitivity is very high. The average sensitivity is 61.3 GHz/mm when d is smaller than 0.5 mm. Furthermore, by changing d, we can realize the tunable THz notch filter reported in [20].

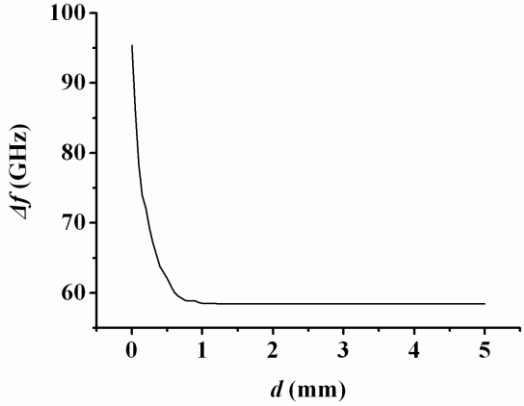

Fig. 7. The dependence of the resonance frequency shift relative to the theoretical value on the interval between the metal plate and PS slab.

When d = 0.3 mm, t = 1 mm, and m = 1, we calculate the dependence of Δf on w, as shown in Fig. 8(a). We can see that the smaller w is, the larger the resonance frequency blueshift is. The blueshifts are 2080 GHz at w = 0.2 mm, and 58 GHz at w = 10 mm, respectively. The maximum frequency-tuning-range caused by w is 2030 GHz, which is 33 times larger than that caused by d (60 GHz) [20]. As we can see in Eq. (8), the blueshift of the resonance frequency is strongly affected by a. When a is very small, the blueshift will be very large and $\Delta f \sim \frac{1}{a}$. When d = 0.3 mm, t = 1 mm, and m = 1, we calculate the mode field distributions for different w, as shown in Fig. 8(b). We can see both l and p will change when w changes. However, their effects are negligible compared with the effects of the changing of w. The phenomenon that the blueshift of resonance frequency increases greatly as w decreases is not discussed in [20], either. The sensitivity of Δf to w is defined as $\Delta(\Delta f)/\Delta w$, where $\Delta(\Delta f)$

and Δ*w* are the variations of Δ*f* and *w*, respectively. When *w* is small enough, the sensitivity is quite high. For example, the sensitivity is 6950 GHz/mm at *w* = 0.2 mm, which is 60 times higher than that reported in [20] (115 GHz/mm). Therefore, by changing *w*, one can realize the tunable THz notch filter with a very large frequency-tuning-range and a very high sensitivity of the resonance frequency shift. Obviously, the higher the sensitivity of the resonance frequency is, the higher the accuracy requirement of the waveguide structure is. In applications, a trade-off between the frequency sensitivity and the structure accuracy requirement should be considered.

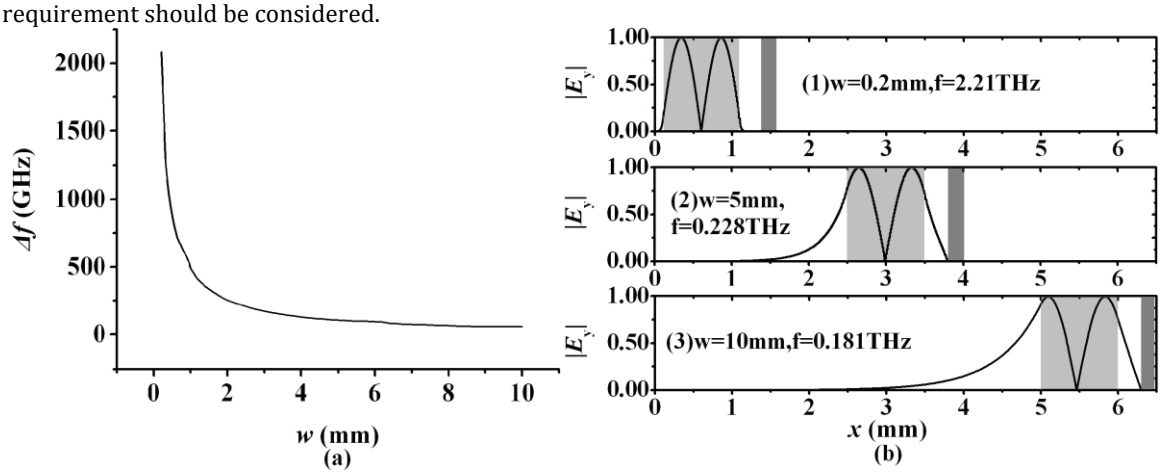

Fig. 8. (a) The dependence of the resonance frequency shift relative to the theoretical value on the interval between the two PS slabs. (b) Mode field distributions for different *w* at *m* = 1. The inset (1) corresponds to *w* = 0.2 mm and f_m = 2.21 THz, the inset (2) corresponds to *w* = 5 mm and f_m = 0.228 THz, and the inset (3) corresponds to *w* = 10 mm and f_m = 0.181 THz.

4. Conclusions

We theoretically study the THz transmission characteristics of the metal-clad antiresonant reflecting hollow waveguides. Base on the dispersion equation derived, we study the effects of the waveguide structure on the resonance frequency in detail. We have also derived the equation for the blueshift of the resonance frequency and find that the blueshift of the resonance frequency is strongly affected by *w*. At *t* = 1 mm, *d* = 0.3 mm, and *m* = 1, by changing *w* we obtain that the maximum frequency-tuning-range is 2030 GHz, which is 33 times larger than that obtained by changing *d* [20]. When *w* = 0.2 mm, *d* = 0.3 mm, and *m* = 1, the maximum sensitivity of the resonance frequency blueshift to *w* is 6950 GHz/mm, which is 60 times larger than that reported in [20]. Moreover, both the loss and the dispersion of the guide modes are very low when the THz wave is far away from the resonance frequency. We believe that these results are of theoretical significance for designing THz filters, sensors and switches.

Acknowledgments

This work was supported in part by the National Natural Science Foundation of China under Grant 61405124, Natural Science Foundation of Guangdong Province, China under Grant 2014A030313560, the Specialized Research Fund for the Doctoral Program of Higher Education of China under Grant 20134408120002, and the Fund Project for Shenzhen Fundamental Research Programme under Grant JCYJ20130329140707824.

Reference

1. G. Gallot, S. P. Jamison, R.W. McGowan, and D. Grischkowsky, "Terahertz waveguides," J. Opt. Soc. Am. B 17, 851-863 (2000).
2. S. Atakaramians, S. Afshar V., T. M. Monro, and D. Abbott, "Terahertz dielectric waveguides" Advances in Optics and Photonics 5, 169–215 (2013).
3. K.Wang, and D. M. Mittleman, "Metal wires for terahertz waveguiding", Nature 432, 376 (2004).
4. K. Wang, and D. M. Mittleman, "Dispersion of surface plasmon polaritons on metal wires in the terahertz frequency range", Phys. Rev. Lett 96, 157401 (2006).
5. T. Jeon, J. Zhang, and D. Grischkowsky, "THz Sommerfeld wave propagation on a single metal wire", Appl. Phys. Lett 86, 161904 (2005).
6. C.-H. Lai, Y.-C. Hsueh, H.-W. Chen, Y.-J. Huang, H.-C. Chang, and C.-K. Sun, "Low-index terahertz pipe waveguides," Opt. Lett. 34, 3457-3459 (2009).
7. C.-H. Lai, B. You, J.-Y. Lu, T.-A. Liu, J.-L. Peng, C.-K. Sun, and H. C. Chang, "Modal characteristics of antiresonant reflecting pipe waveguides for terahertz waveguiding," Opt. Express 18, 309-322(2010).
8. J.-T. Lu, Y.-C. Hsueh, Y.-R. Huang, Y.-J. Hwang, and C.-K. Sun, "Bending loss of terahertz pipe waveguides," Opt. Express 18, 26332–26338 (2010).

9. E. Nguema, D. Fèrachou, G. Humbert, J. L. Auguste, and J. M. Blondy, "Broadband terahertz transmission within the air channel of thin-wall pipe," Opt. Lett. 36, 1782–1784 (2011).
10. H. W. Liang, S. C. Ruan, M. Zhang, H. Su and I. L. Li, "Surface plasmon-polaritons on very thin metal tubes" Opt. Express 23, 125001 (2013).
11. S. Kaijage, Z. Ouyang, X. Jin, "Porous-Core Photonic Crystal Fiber for Low Loss Terahertz Wave Guiding," IEEE Photo. Tech. Lett. **25**(15), 1454-1457, (2013).
12. N.-N. Chen, J. Liang, L. Ren, "High-birefringence, low-loss porous fiber for single-mode terahertz-wave guidance," Appl. Opt. **52**(21), 5297-302, (2013).
13. S. Li, H. Zhang, J. Bai, W. Liu, Z. Jiang, and S. Chang, "Dual-Porous Fiber-Based Low Loss Broadband Terahertz Polarization Splitter" IEEE Photo. Tech. Lett. 26(14), 1399-1402, (2014).
14. T. Ma, A. Markov, L. Wang, and M. Skorobogatiy, "Graded index porous optical fibers – dispersion management in terahertz range" Opt. Express 23(6), 7856-7869, (2015).
15. I. J. H. McCrindle, J. Grant, T. D. Drysdale, and D. R. S. Cumming, "Hybridization of optical plasmonics with terahertz metamaterials to create multi-spectral filters," Opt. Express 21(16), 19142-19152 (2013).
16. H. T. Chen, J. F. O'Hara, A. J. Taylor, R. D. Averitt, C. Highstrete, M. Lee, and W. J. Padilla, "Complementary planar terahertz metamaterials," Opt. Express 15(3), 1084-1095 (2007).
17. H.-T. Chen, W. J. Padilla, J. M. O. Zide, S. R. Bank, A. C. Gossard, A. J. Taylor, and R. D. Averitt, "Ultrafast optical switching of terahertz metamaterials fabricated on ErAs/GaAs nanoisland superlattices," Opt. Lett. 32(12), 1620–1622 (2007).
18. H. Zhang, P. Guo, P. Chen, S. Chang, and J. Yuan, "Liquid-crystal-filled photonic crystal for terahertz switch and filter," J. Opt. Soc. Am. B 26(1), 101–106 (2009).
19. R. Mendis, A. Nag, F. Chen, and D. M. Mittleman, "A tunable universal terahertz filter using artificial dielectrics based on parallel-plate waveguides," Appl. Phys. Lett. 97(13), 131106 (2010).
20. J.-Y. Lu, H.-Z. Chen, C.-H. Lai, H.-C. Chang, B. You, T.-A. Liu, and J.-L. Peng, "Application of metal-clad antiresonant reflecting hollow waveguides to tunable terahertz notch filter," Opt. Express 19(1), 162–167 (2011).
21. B. S. Phillips, P. Measor, Y. Zhao, H. Schmidt, and A. R. Hawkins, "Optofluidic notch filter integration by lift-off of thin films," Opt. Express 18(5), 4790–4795 (2010).
22. B. You, J.-Y. Lu, J.-H. Liou, C.-P. Yu, H.-Z. Chen, T.-A. Liu, and J.-L. Peng, "Subwavelength film sensing based on terahertz anti-resonant reflecting hollow waveguides," Opt. Express 18(18), 19353–19360 (2010).
23. B. You, J.-Y. Lu, C.-P. Yu, T.-A. Liu, and J.-L. Peng, "Terahertz refractive index sensors using dielectric pipe waveguides," Opt. Express 20(6), 5858–5866 (2012).
24. R. Mendis, V. Astley, J. Liu, and D. M. Mittleman, "Terahertz microfluidic sensor based on a parallel-plate waveguide resonant cavity," Appl. Phys. Lett. 95 (17), 171113 (2009).
25. S. Harsha, N. Laman, and D. Grischkowsky, "High-Q terahertz Bragg resonances within a metal parallel plate waveguide," Appl. Phys. Lett. 94(9), 091118 (2009).
26. W. Zhu, A. Agrawal, and A. Nahata, "Planar plasmonic terahertz guided-wave devices," Opt. Express 16(9), 6216–6226 (2008).
27. R. Mendis and D. M. Mittleman, "An investigation of the lowest-order transverse-electric (TE1) mode of the parallel-plate waveguide for THz pulse propagation," J. Opt. Soc. Am. B 26, A6-A13 (2009).
28. R. Mendis and D. M. Mittleman, "Comparison of the lowest-order transverseelectric (TE1) and transverse-magnetic (TEM) modes of the parallel-plate waveguide for terahertz pulse applications," Opt. Express 17, 14839-14850 (2009).
29. J. Liu, H. Liang, M. Zhang, and H. Su, "Broadband terahertz transmission within the symmetrical plastic film coated parallel-plate waveguide" App. Opt. 53(26), 6008-6012 (2014).
30. H. W. Liang, S. C. Ruan, M. Zhang, H. Su and I. L. Li , "Characteristics of modified surface plasmon polaritons on double-coated metal nanofilms" Laser Phys. Lett. 11, 115003 (2014).
31. M. Gong, T.-I. Jeon, and D. Grischkowsky, "THz surface wave collapse on coated metal surfaces" Opt. Express 17(19), 17088-17101 (2009).
32. J. Saxler, J. G. Rivas, C. Janke, H. P. M. Pellemans, P. H. Bolı´var, and H. Kurz, "Time-domain measurements of surface plasmon polaritons in the terahertz frequency range" Phys. Rev. B 69, 155427 (2004).
33. T. H. Isaac,W. L. Barnes, and E. Hendry, "Determining the terahertz optical properties of subwavelength films using semiconductor surface plasmons" Appl. Phys. Lett. 93, 241115 (2008).
34. J. Liu, H. Liang, M. Zhang, and H. Su, "Metal plate for guiding terahertz surface plasmon-polaritons and its sensing applications" Opt. Communications **339** 222–227 (2014).
35. M. A. Duguay, Y. Kokubun, T. L. Koch, and L. Pfeiffer, "Antiresonant reflecting optical waveguides in SiO2-Si multilayer structures," Appl. Phys. Lett. 49 (1), 13–15 (1986).
36. A. Yariv, Optical Electronics in Modern Communications (Oxford U. Press, Oxford, 2007).
37. M. A. Ordal, R. J. Bell, R. W. Alexander, Jr, L. L. Long, and M. R. Querry, "Optical properties of fourteen metals in the infrared and far infrared: Al, Co, Cu, Au, Fe, Pb, Mo, Ni, Pd,Pt, Ag, Ti, V, and W," Appl. Opt. 24(24), 4493–4499 (1985).
38. J. R. Birch, "The far-infrared optical constants of polypropylene, PTFE, and polystyrene," Infrared Phys. 33(1), 33–38, (1992).